Optics Letters

Efficient middle-infrared generation in $LiGaS_2$ by simultaneous spectral broadening and difference-frequency generation

B.-H. Chen,[1,2] T. Nagy,[3] and P. Baum[1,2,*]

[1]Ludwig-Maximilians-Universität München, Am Coulombwall 1, 85748 Garching, Germany
[2]Max-Planck-Institute of Quantum Optics, Hans-Kopfermann-Str. 1, 85748 Garching, Germany
[3]Max Born Institute for Nonlinear Optics and Short Pulse Spectroscopy, Max-Born-Str. 2A, 12489 Berlin, Germany
*Corresponding author: peter.baum@lmu.de

Received 17 January 2018; accepted 6 March 2018; posted 13 March 2018 (Doc. ID 319975); published 10 April 2018

We report a surprisingly broadband and efficient midinfrared pulse generation in $LiGaS_2$ (Langasite, LGS) by invoking a simultaneous interplay of intrapulse difference-frequency generation, self-phase modulation, and dispersion. This cascaded mechanism expands the output bandwidth and output power at the same time. With 30-fs driving pulses centered at 1030-nm wavelength we obtain a broadband middle-infrared spectrum of 8–11 μm with an LGS crystal as thick as 4 mm, which is eight times longer than the walk-off length.

OCIS codes: (140.3070) Infrared and far-infrared lasers; (140.3538) Lasers, pulsed; (190.4223) Nonlinear wave mixing; (320.7110) Ultrafast nonlinear optics.

https://doi.org/10.1364/OL.43.001742

Short and broadband optical pulses at midinfrared (MIR) or multiterahertz (THz) frequencies have a key importance in various research fields. They are, for example, essential for molecular fingerprint spectroscopy [1–3], all-optical electron pulse compression [4], and high-field experiments in condensed matter [5–7]. A common way to produce MIR few-cycle pulses is intrapulse difference-frequency generation (DFG) [8–11] in a nonlinear crystal. This nonlinear optical mechanism is related to optical rectification and produces broadband, low-frequency electromagnetic radiation at a center frequency that is approximately given by the available spectral width of the pump pulses.

In practice, however, there are not many optical materials with high nonlinear coefficients in the relevant spectral ranges, and often there is also velocity mismatch between the MIR radiation and driving optical pulses. One of the more favorable materials is $LiGaS_2$ (Langasite, LGS). Although its effective nonlinearity is rather low ($d_{\mathrm{eff}} \approx 5.8$ pm/V), the material has on the other hand a wide transparency range (about 0.32 to 11.6 μm), a high damage threshold, and a particularly weak two-photon absorption when excited with femtosecond pulses at >600 nm wavelength (bandgap ≈ 4.15 eV). However, temporal walk-off between the two required driving polarizations along the ordinary (o) and extraordinary (e) axes limits the overall efficiency and spectral bandwidth of the MIR output. For example, for 30-fs driving pulses at 1030 nm wavelength, there is less than 0.45 mm of LGS crystal that will be efficient. The conversion efficiency suffers accordingly.

To our surprise, we found in experiments with the setup depicted in Fig. 1 that even with an eight times longer crystal than the walk-off length, MIR generation is still highly efficient and particularly broadband. In this Letter, we argue that the temporal walk-off is continuously compensated by nonlinear spectral broadening and dispersion of the driving pulses during propagation, in such a way that the high-frequency components of the extraordinary/faster part of the pump pulse and the low-frequency component of the ordinary/slower part of the pump pulse have a continuous overlap all the time.

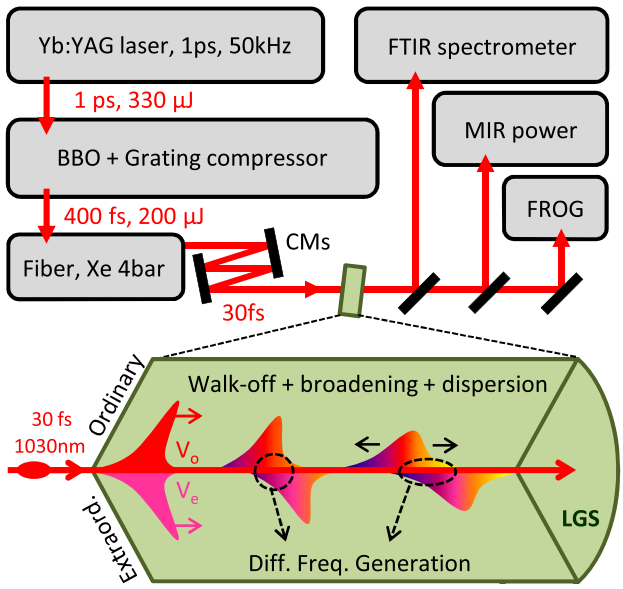

Fig. 1. Experimental setup and concept for simultaneous, cascaded spectral broadening and intrapulse DFG. Yb:YAG, ytterbium-doped yttrium aluminum garnet; FTIR, Fourier-transform infrared spectroscopy.

This mechanism (depicted in the lower part of Fig. 1) allows using substantially longer crystals than expected, for example 4 mm instead of 0.45 mm at our experimental conditions, in order to simultaneously achieve higher MIR frequencies and more output power. The following data shall support this interpretation and establish the concept for future applications.

In the experiment (see Fig. 1), 1.0-ps pulses from a regenerative thin-disk laser [12] (1030 nm wavelength, 330 μJ pulse energy, 50 kHz repetition rate, 16.5 W output average power) are first compressed via cascaded $\chi^{(2)}$ broadening [13–16] in a β-barium-borate (BBO) crystal and a grating compressor (1000 lines/mm) to a pulse duration of 400 fs. In a second stage, these 400-fs pulses are coupled into a 2.7-m long stretched flexible hollow fiber [17,18] with 320 μm inner diameter filled with 4 bar xenon; these results are reported in more detail elsewhere [19]. The spectrally broadened output pulses are compressed by 20 bounces on double-angled chirped mirrors down to 30-fs pulse duration. Results of second-harmonic-generation frequency-resolved optical gating (SHG-FROG, error 0.65%) are reported in Fig. 2 and reveal 30-fs pulses with low pedestals in time. More than 60 μJ of pulse energy or 3 W of average power was available in this way. A maximum pulse energy of 20 μJ is used in all the measurements described in order to avoid crystal damage. These 30-fs pulses have a spectrum from 970 to 1095 nm at 1% level. Difference-frequency generation between these extreme components should allow producing MIR pulses with a spectrum extending down to 8.5 μm.

We begin our report on the physics within LGS by measuring the output MIR spectrum by a Fourier-transform spectrometer (L-FTS, LASNIX GmbH) in dependence of the input power with a 4-mm long LGS crystal ($\theta = 90°$, $\varphi = 38.5°$, Ascut Ltd.). In order to satisfy type II phase matching (e + o → e), the crystal is rotated around the beam axis by 45° in such a way that the input p-polarization sees the two crystal axes (e and o) with equal contribution. According to the linear-optical walk-off between the two active crystal axes,

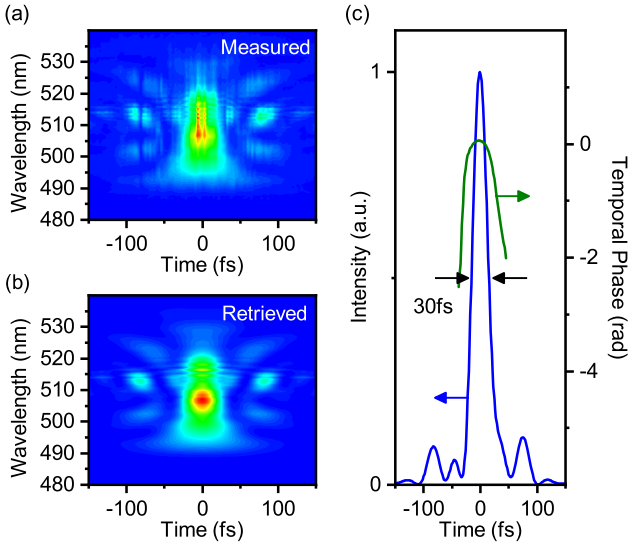

Fig. 2. SHG-FROG of the driving 30-fs laser pulse from a hollow-core fiber. (a) Measured FROG trace. (b) Retrieved FROG trace. (c) Retrieved temporal pulse shape. FROG error, ~0.65%.

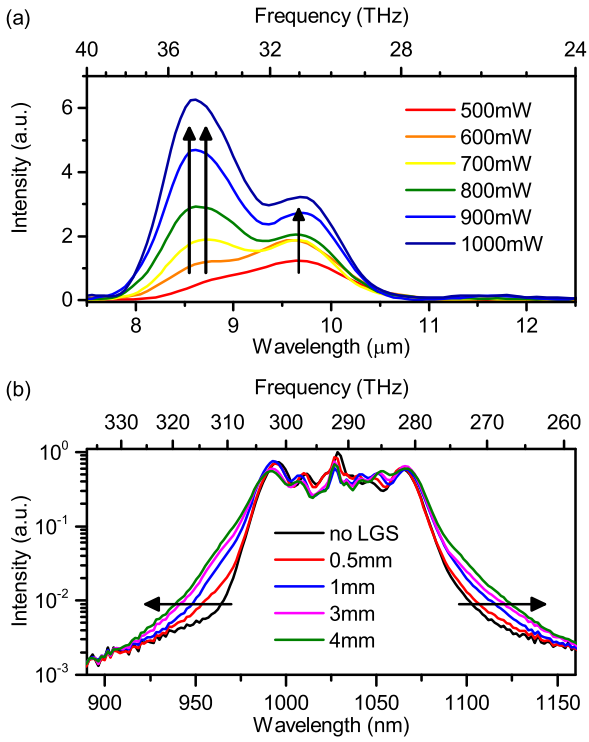

Fig. 3. Evidence in the spectral domain. (a) MIR spectra with different input power. (b) Optical spectrum for different thicknesses of the LGS crystal.

about 67.4 fs/mm, this crystal is eight times longer than useful for our 30-fs pump pulses (see Fig. 2).

Figure 3(a) shows the MIR spectrum generated in the 4-mm LGS crystal as a function of increasing input power. While there is the expected increase of output power, the striking observation is a substantial reshaping of the output spectrum. The intensity increase in the short-wavelength region (7–8.6 μm) is much stronger than in the longer-wavelength part [Fig. 3(a), black arrows]. This is a first strong indication that more nonlinear processes than only DFG or optical rectification are at work.

More direct evidence for the above-mentioned mechanism is reported in Fig. 3(b). We measured the spectrum of the 30-fs pump pulses after propagation through four different thicknesses of LGS crystal at otherwise identical conditions (1 W, 130 GW/cm^2). The spectrum of the transmitted pulses becomes symmetrically broader on both sides for longer crystals. This excludes substantial influences from cascaded difference-frequency mixing [20] and rather indicates the presence of self-phase modulation [21,22]. The broadening starts to saturate at around 4 mm thickness [compare in Fig. 3(b) the magenta and green traces], because the dispersion of the optical pulses (~300 fs^2/mm) eventually lowers their intensity.

Having a broadened pump spectrum is still not yet enough to explain the unusually broadband MIR spectra of Fig. 3(a); the new components also need to overlap in time. Figure 4 shows the results of SHG-FROG measurements of the pump pulse shapes after passage through the 4-mm LGS crystal. The FROG device is based on a 80-μm-thick BBO crystal that is oriented such that the projection of both output polarizations of the LGS crystal are measured (optical axis at 45° to the LGS

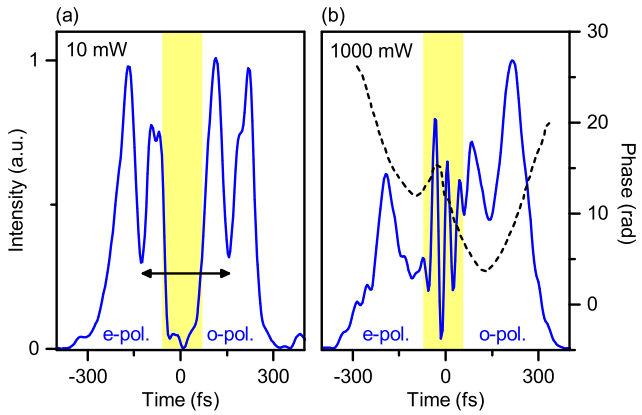

Fig. 4. Evidence in the temporal domain. Retrieved FROG pulse shape with an input power of (a) 10 mW and (b) 1000 mW. Yellow, region around time zero. Dashed line, retrieved phase.

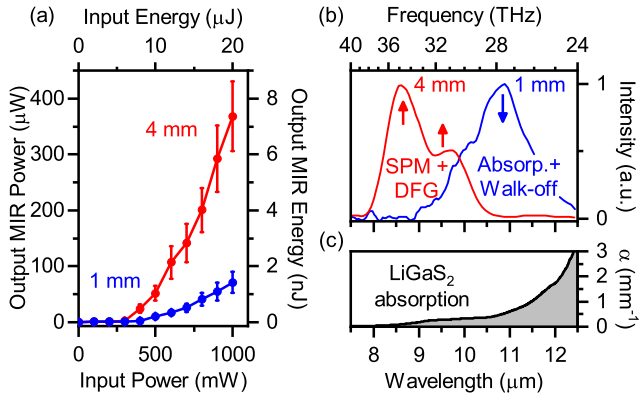

Fig. 5. Overall performance. (a) Output power with a 1-mm (blue) and a 4-mm (red) LGS crystal. (b) MIR spectrum generated from a 1-mm (blue) and a 4-mm (red) LGS crystal. (c) Measured linear absorption curve of our LGS material.

axis) simultaneously. Figure 4(a) shows a measurement at very low input power (10 mW), where no spectral broadening can occur. We see that the pump pulses split in time into two distinct envelopes, due to the expected walk-off in birefringent LGS, as explained previously. The measured walk-off is about 300 fs for our crystal (black arrow). The two polarizations are fully separated after the LGS, and at the later part of the crystal there is no possibility for DFG. Figure 4(a) also reveals directly in the time domain the expected linear-optical dispersion of each crystal axis, which transforms the double-lobed 30-fs pump pulse spectrum [compare Fig. 3(b)] into the measured double-lobed time structures.

In contrast, when a higher input power of 1 W, 130 GW/cm^2 is applied [see Fig. 4(b)], the mechanism of Fig. 1 kicks in and the two parts of the pump pulses suffer broadening and more dispersion in the crystal. As seen in Fig. 4(b), both polarizations become longer in time. Intriguingly, there is now still temporal overlap, even interference, after passage through the crystal. The two polarizations from the two LGS axes are still interacting with each other even after 4 mm of LGS. Because of the positive dispersion experienced by the optical pulse, the blue part of the e-polarized pulse overlaps with the red part of the o-polarized pulse in a very beneficial way for high-frequency MIR generation. The FROG's beamsplitter had different transmission for e- and o- polarization, and this effect was corrected in Fig. 4. The period (peak to peak) of the oscillation in the overlapping region (yellow) is roughly 30 fs and shows the coherence between the different polarization components after 45° selection.

In a final measurement, we compared the overall performance of 1-mm and a 4-mm LGS crystals. Figure 5(a) shows the power dependence of these two crystals. These data were obtained by measuring the power after an uncoated germanium (Ge) near-infrared filter and corrected by taking Fresnel losses into account (40% transmission for normal incidence). As one would expect from a $\chi^{(2)}$ process, a quadratic-like power dependence is measured, but the 4-mm crystal performs substantially better (0.037% power conversion, 0.32% quantum efficiency). This conversion efficiency is five times lower than previously reported at three times higher peak intensity [9]. Therefore, if assuming a quadratic intensity dependence of the overall cascaded mechanism, our 4-mm crystal performs better. We did not want to apply the audacious 350 GW/cm^2 of [9] to our crystals, in order to avoid damage. Nanojoule pulse energies and MV/m E-fields, as now available at 7.5–11 μm, are sufficient for our intended applications in femtosecond and attosecond electron microscopy [4,23,24], but also for many other applications.

Figure 5(b) shows the two MIR spectra at 1 W pump power. For the 1-mm LGS crystal, there are no high-frequency components below 9 μm wavelength and the strongest output is around 10.5 μm. In contrast, for the 4-mm LGS, there are substantially more high-frequency components at wavelengths down to 7.5 μm. Figure 5(c) shows our LGS crystals' absorption curve, measured with a FTS (Bruker Corp.). The crystals have a substantial absorption above 11 μm, explaining the reduction of low-frequency components in case of the 4-mm crystal.

Overall, there emerges the picture that was outlined above (see Fig. 1, lower part). At the beginning of the crystal, the pump pulses decompose into two orthogonally polarized parts along the two LGS axes. Both parts are stretching in time and also temporally walk away from each other due to dispersion and group velocity mismatch. In the first 0.5–1 mm, nonlinear spectral broadening and absorption are not yet substantial. The resulting MIR spectrum is shown as the blue curve in Fig. 5(b). As the pump pulses propagate further into the 4-mm crystal, self-phase modulation leads to broader spectra and the dispersion together with walk-off keep the bluest and reddest parts in continuous overlap. Consequently, more MIR power is produced and the shortest MIR wavelengths are created preferentially, while wavelengths beyond 11 μm are gradually absorbed.

We conclude with three remarks. First, in a way, our reported combination of nonlinear-optical self-phase modulation with nonlinear-optical difference-frequency mixing is one more example of cascaded or multiprocess nonlinear optics [25–27]. Second, it seems clear now why somewhat broader MIR spectra than expected have been reported before [9]. Third, there should be other optical materials for which this picture also applies, namely whenever self-phase modulation and dispersion create enough temporal effects to compete with walk-off. Novel optical applications might be ahead.

Funding. Munich Centre of Advanced Photonics; H2020 European Research Council (ERC) (DIVI).

REFERENCES

1. A. Schliesser, N. Picqué, and T. W. Hänsch, Nat. Photonics **6**, 440 (2012).
2. F. Adler, M. J. Thorpe, K. C. Cossel, and J. Ye, Annu. Rev. Anal. Chem. **3**, 175 (2010).
3. C. Y. Wang, T. Herr, P. Del'Haye, A. Schliesser, J. Hofer, R. Holzwarth, T. W. Hänsch, N. Picqué, and T. J. Kippenberg, Nat. Commun. **4**, 1345 (2013).
4. C. Kealhofer, W. Schneider, D. Ehberger, A. Ryabov, F. Krausz, and P. Baum, Science **352**, 429 (2016).
5. S. Ghimire, A. D. DiChiara, E. Sistrunk, P. Agostini, L. F. DiMauro, and D. A. Reis, Nat. Phys. **7**, 138 (2011).
6. O. Schubert, M. Hohenleutner, F. Langer, B. Urbanek, C. Lange, U. Huttner, D. Golde, T. Meier, M. Kira, S. W. Koch, and R. Huber, Nat. Photonics **8**, 119 (2014).
7. M. Hohenleutner, F. Langer, O. Schubert, M. Knorr, U. Huttner, S. W. Koch, M. Kira, and R. Huber, Nature **523**, 572 (2015).
8. K. Kaneshima, N. Ishii, K. Takeuchi, and J. Itatani, Opt. Express **24**, 8660 (2016).
9. I. Pupeza, D. Sánchez, J. Zhang, N. Lilienfein, M. Seidel, N. Karpowicz, T. Paasch-Colberg, I. Znakovskaya, M. Pescher, W. Schweinberger, V. Pervak, E. Fill, O. Pronin, Z. Wei, F. Krausz, A. Apolonski, and J. Biegert, Nat. Photonics **9**, 721 (2015).
10. M. Knorr, J. Raab, M. Tauer, P. Merkl, D. Peller, E. Wittmann, E. Riedle, C. Lange, and R. Huber, Opt. Lett. **42**, 4367 (2017).
11. T. Morimoto, N. Sono, T. Miyamoto, N. Kida, and H. Okamoto, Appl. Phys. Express **10**, 122701 (2017).
12. W. Schneider, A. Ryabov, C. Lombosi, T. Metzger, Z. Major, J. A. Fülöp, and P. Baum, Opt. Lett. **39**, 6604 (2014).
13. R. DeSalvo, H. Vanherzeele, D. J. Hagan, M. Sheik-Bahae, G. Stegeman, and E. W. Van Stryland, Opt. Lett. **17**, 28 (1992).
14. M. Seidel, J. Brons, G. Arisholm, K. Fritsch, V. Pervak, and O. Pronin, Sci. Rep. **7**, 1410 (2017).
15. R. Šuminas, G. Tamošauskas, V. Jukna, A. Couairon, and A. Dubietis, Opt. Express **25**, 6746 (2017).
16. X. Liu, L. J. Qian, and F. Wise, Opt. Lett. **24**, 1777 (1999).
17. T. Nagy, M. Forster, and P. Simon, Appl. Opt. **47**, 3264 (2008).
18. T. Nagy, V. Pervak, and P. Simon, Opt. Lett. **36**, 4422 (2011).
19. B. Chen, M. Kretschmar, D. Ehberger, A. Blumenstein, P. Simon, P. Baum, and T. Nagy, Opt. Express **26**, 3861 (2018).
20. A. M. Weiner, J. P. Heritage, and R. H. Stolen, J. Opt. Soc. Am. B **5**, 364 (1988).
21. D.-P. Wei, T. V. Galstian, I. V. Smolnikov, V. G. Plotnichenko, and A. Zohrabyan, Opt. Express **13**, 2439 (2005).
22. Q. Z. Wang, Q. D. Liu, D. Liu, P. P. Ho, and R. R. Alfano, J. Opt. Soc. Am. B **11**, 1084 (1994).
23. A. Ryabov and P. Baum, Science **353**, 374 (2016).
24. Y. Morimoto and P. Baum, Nat. Phys. **14**, 252 (2018).
25. C. Manzoni, G. Cerullo, and S. De Silvestri, Opt. Lett. **29**, 2668 (2004).
26. C. Homann, M. Bradler, M. Förster, P. Hommelhoff, and E. Riedle, Opt. Lett. **37**, 1673 (2012).
27. H. Fattahi, A. Schwarz, S. Keiber, and N. Karpowicz, Opt. Lett. **38**, 4216 (2013).